IEEE P2716 Board Level Shielding Round Robin Measurements

A C Marvin, H Xie, J F Dawson, L Dawson, J Yan
University of York
December 2019

Introduction.

This report describes reverberation chamber measurements undertaken at the University of York (UoY) in the IEEE P2716 round-robin Board-level Shielding (BLS) measurement programme.

Two SE definitions, Unstirred SE and Stirred SE, are described and both types of SE measurements on the sample shields are presented. The available dynamic range of each technique is established.

1. Measurement methodology

1.1 Reverberation chamber

All of the measurements were conducted in the UoY reverberation chamber which has dimensions 4.7m×3.0m×2.37m ($L \times W \times H$). It has a large stirrer, optimized for low frequency performance as described in [1] and a lowest useable frequency of 200MHz. Connectors panels are available in several places on the wall. Figure 1, below shows the interior of the York chamber with the connector panel to the left, the measurement jig used in this study centre and the stirrer and antenna [2] in the background.

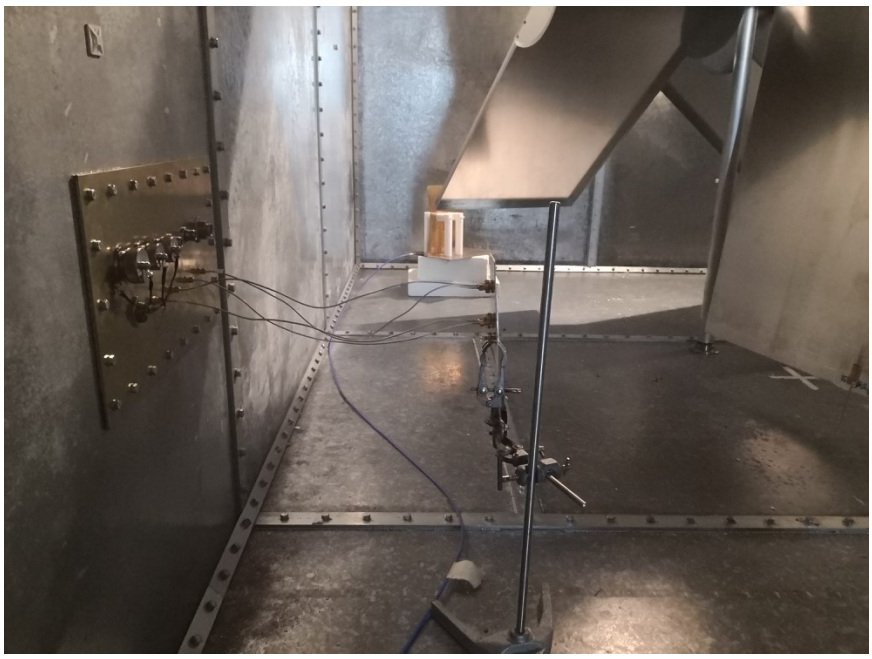

Figure 1. UoY Reverberation chamber

1.2 Board Level Shielding jig

A jig was fabricated using a piece of double sided copper clad printed circuit board (PCB) laminate. SMA connectors were used to mount three strip-lines manufactured from brass sheet. The characteristic impedance of each strip-line is 50Ω and each has a length of 25mm. The shield to be measured is soldered to the board above Shield strip-line. The second stripline is parallel to the Shield strip-line with a spacing of 50mm and the third is orthogonal to the Shield strip-line and 50mm from its centre. See Figures 2, 3, 4 and 5 below.

These dimensions are chosen to be representative of the typical application of a board level shield. The strip-lines represent typical circuit elements found around and within such a shield. Fig 4 shows a side view of the jig. The SMA connectors' outer conductors are extended with 8mm long brass tubes fitted over the extended dielectric and inner conductor to form an extended coaxial transmission line. This transmission line passes through the double sided PCB and is soldered onto the copper ground plane on the side with the strip-lines to which the shield is soldered. This structure ensures that no energy can propagate into the jig through waves guided in the PCB dielectric between the two sided copper cladding.

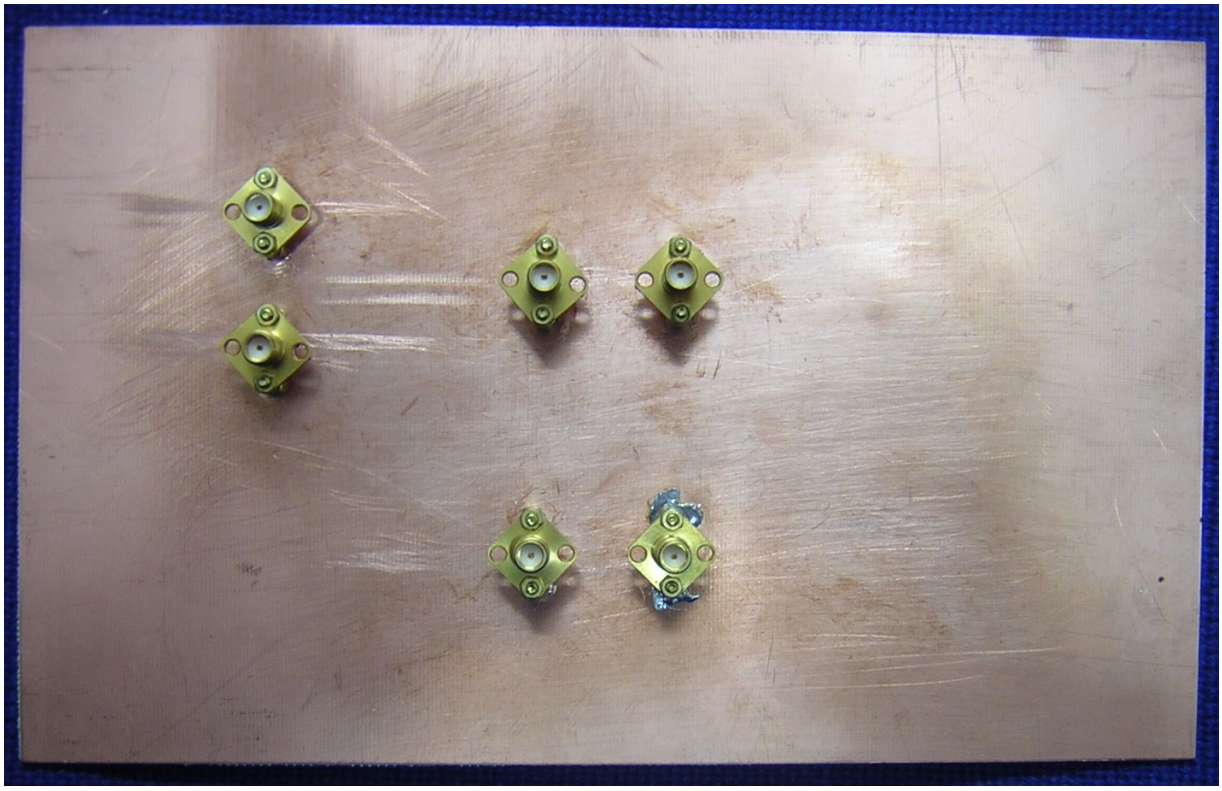

Figure 2. UoY jig – connector side

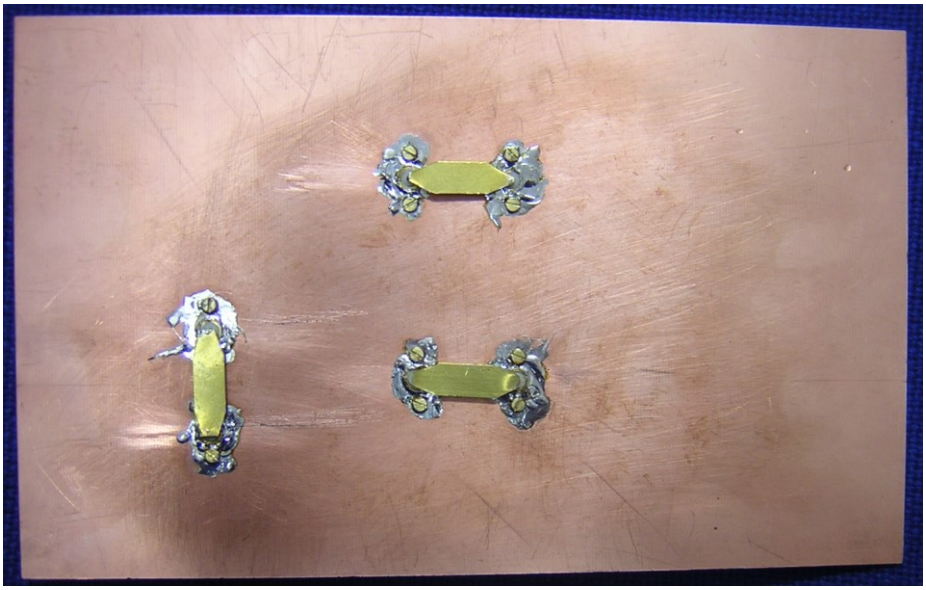

Figure 3. UoY jig – measurement side

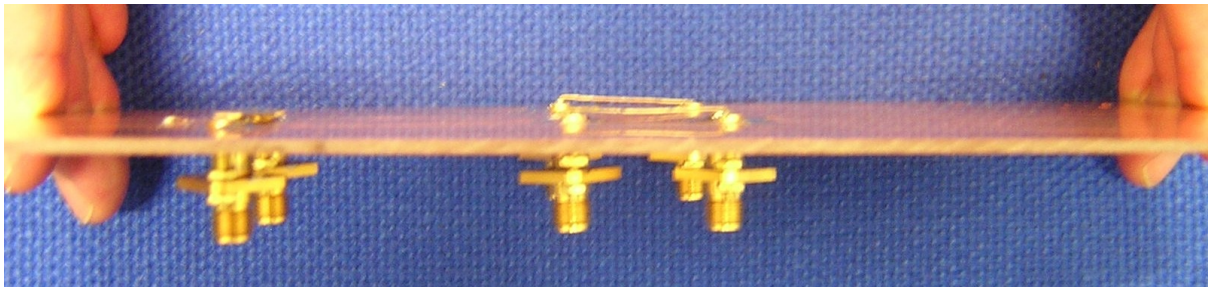

Figure 4. UoY Jig side view

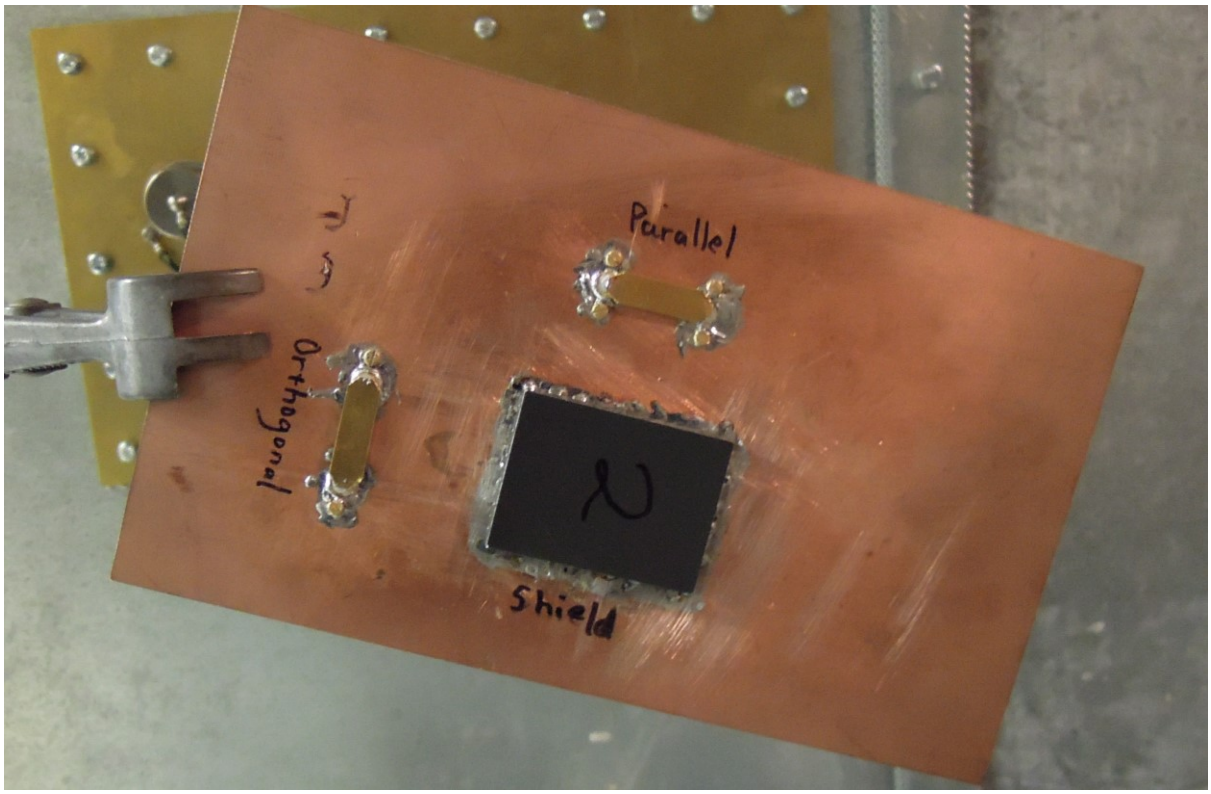

Figure 5. UoY Jig with a Shield attached.

1.3 Measurement setup

A R&S ZVB20 vector network analyser was used for all measurements. The measurement frequency range was from 200MHz to 20GHz with 397 frequency points giving a 50MHz frequency increment. The stirrer was rotated through one complete rotation for each measurement with 100 stirrer positions.

Strip-lines not in use in a measurement were left with open-circuit terminations. Strip-lines used were connected at one end to the VNA with the other end terminated with a 50Ω SMA load. Initial experiments indicated no significant directional differences on the strip-line coupling.

A measure of the shielding effectiveness of the board level shield can therefore be determined using coupling to the Shield strip-line from an external antenna, or from the parallel or orthogonal external strip-lines. Measurements being taken with and without the board level shield in place covering the Shield strip-line.

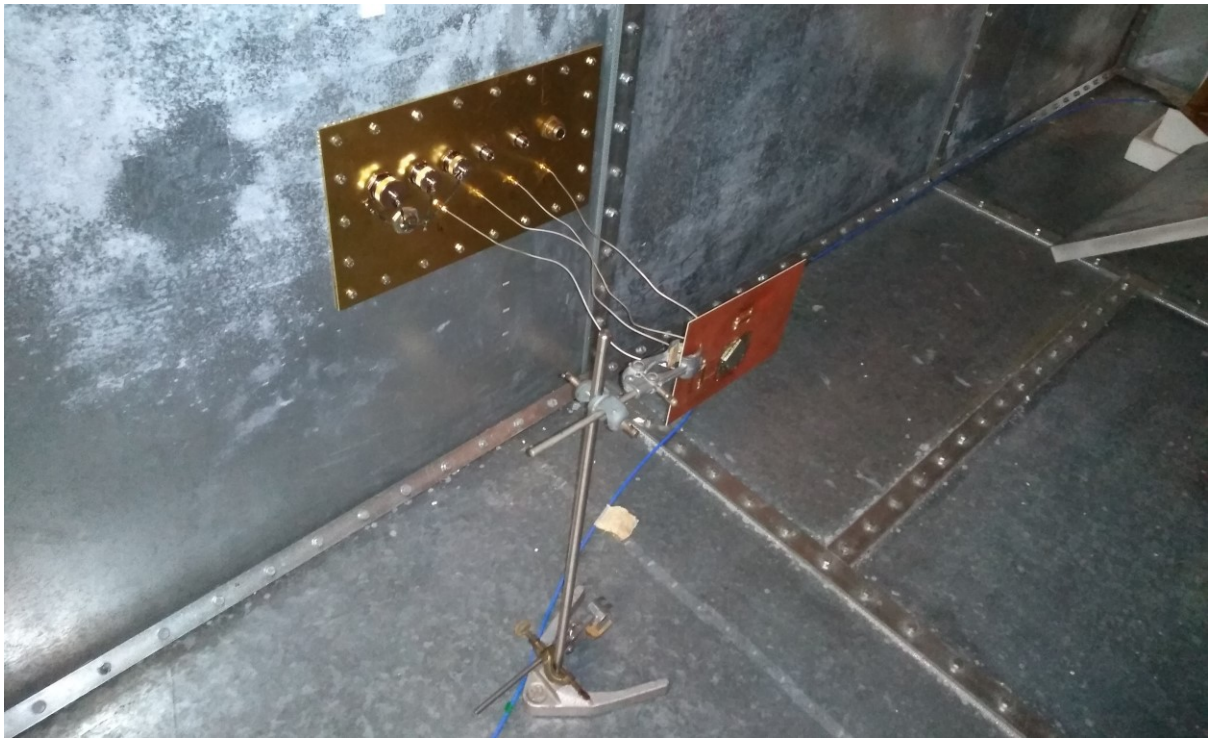

Figure 6. Showing the measurement jig supported using a retort stand and connected using semi-rigid cables to the connector panel

1.4 Data processing

The shielding effect of the board level shields was derived by measuring the S21 parameter between the shield strip-line and the antenna, the parallel strip-line and the orthogonal strip-line.

Initial measurements indicated that the S11 and S22 parameters for all measurements were sufficiently well matched to make corrections for these parameters unnecessary.

The measurement dynamic range available was determined by removing the semi-rigid cable from the shield strip-line and terminating it with a matched load. This load was then placed in contact with the shield strip-line connector. In this way the geometry of the measurement

system was preserved. The S21 parameter was measured with this set-up to assess the measurement noise and spurious coupling level. A measurement bandwidth of 10kHz and a source power level of 20dBm was found to give adequate dynamic range without an excessive measurement time.

The Shielding Effectiveness is measured from coupling to the shield strip-line from the antenna in the chamber. This represents a conventional view of the shielding. The Shielding Effectiveness is also measured from coupling to the shield strip-line from the parallel and orthogonal strip-lines. These measurements represent a more realistic coupling environment for the shield where shielding is required from adjacent sources on the same circuit board. In this case the role of the reverberation chamber is to mimic the range of reflective environments that the board level shield may be exposed to by the likely presence of a reflective equipment enclosure around the board level shield.

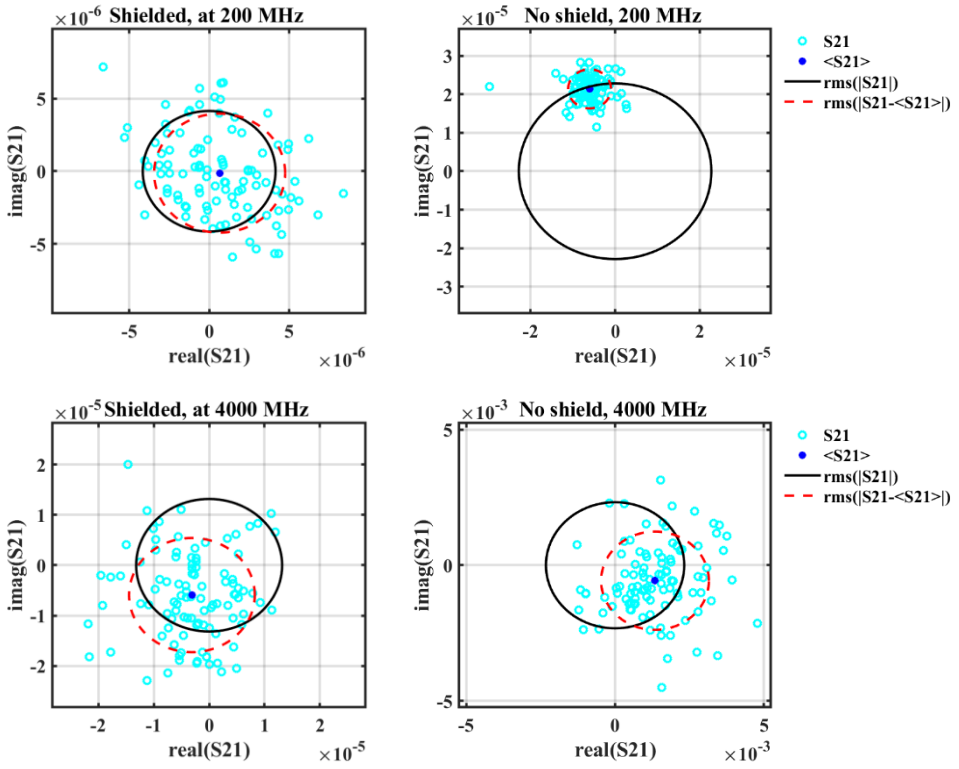

Figure 7. Typical Scatter plots of S21 at 200MHz and 4GHz.

Fig. 7 shows typical scatter plots of the complex S21, in this case for Shield Sample 1 coupling from the orthogonal strip-line, at example frequencies of 200MHz and 4GHz. The individual points (open circles) are the 100 stirrer positions. The spot is the phasor average ($\langle S_{21} \rangle$) of these and represents the unstirred coupling. The circles show the rms magnitude of the S21 data ($\mathrm{rms}(S_{21})$) and for the centered S21 data after the unstirred component is removed ($\mathrm{rms}(S_{21} - \langle S_{21} \rangle)$). It can be seen that there is a substantial difference between these at 200 MHz.

Two definitions of Shielding Effectiveness have been established.

1.4.1 Unstirred Shielding Effectiveness

Unstirred shielding effectiveness is derived from the stationary or unstirred components of the coupling between the shield strip-line and the other strip-lines or the antenna.

The S21 parameter is measured with and without the shield present and, at each frequency, the ratio of the phasor (vector) averages of these measurements over the 100 stirrer positions is the Unstirred SE. This is the ratio of the moduli of the 'spots' in Fig 7.

The unstirred dynamic range is evaluated by repeating the above but replacing the shield measurement with the matched load.

Unstirred Shielding Effectiveness represents the direct coupling between the source and the shield interior.

1.4.2 Stirred Shielding Effectiveness

Stirred Shielding Effectiveness is derived from the stirred components of the coupling between the shield strip-line and the other strip-lines or the antenna. The unstirred component (vector or phasor average over the stirrer rotation, 'spots' in Fig 7) of the S21 measurements at each frequency were subtracted from the S21 measurements leaving the stirred components. The ratio of the average of the mean square scalar magnitudes of the stirred S21 measurements over the stirrer rotation with and without the shield present then represents the Stirred SE.

The stirred dynamic range is evaluated from the ratio of these data without the shield present to the data with the shield strip-line cable terminated in a matched load.

Stirred Shielding Effectiveness represents the coupling between the source and the shield interior through reverberant energy. This coupling mimics the situation where the board level shield is enclosed within a larger equipment enclosure that is reverberant.

2. Dynamic range

The dynamic range data for the measurement set-up are shown in Figures 8 and 9 below. In general the dynamic range is above 50dB. The exception is the dynamic range of the stirred Shielding Effectiveness measurements for the parallel and orthogonal strip-line coupling. To date we have no definitive explanation for these results which exhibit a significantly lower dynamic range, particularly below 2GHz.

In order to maintain the dynamic range great care has to be taken with the measurements. In particular, the integrity of the solder connections on the jig and the semi-rigid cables connecting the jig to the connector panel within the chamber must be maintained. Careful visual inspection of solder joints on the jig is recommended between each test involving soldering or unsoldering test samples. All SMA connectors inside the chamber should be tightened with a torque spanner whenever a change is made on the jig.

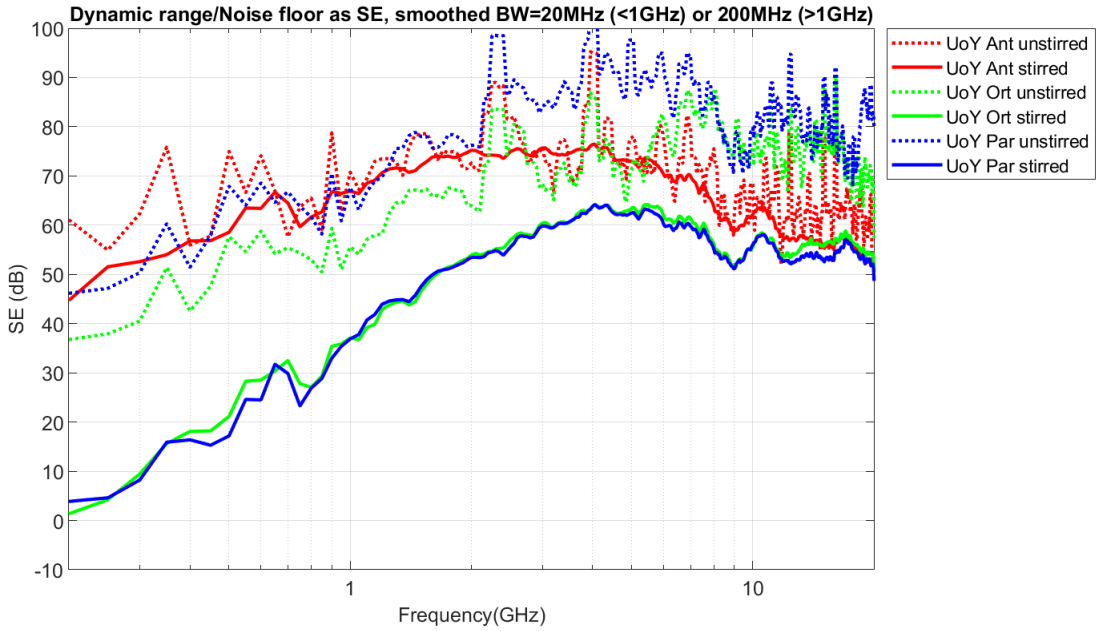

Figure 8. Dynamic range for the different measurement techniques (log scale)

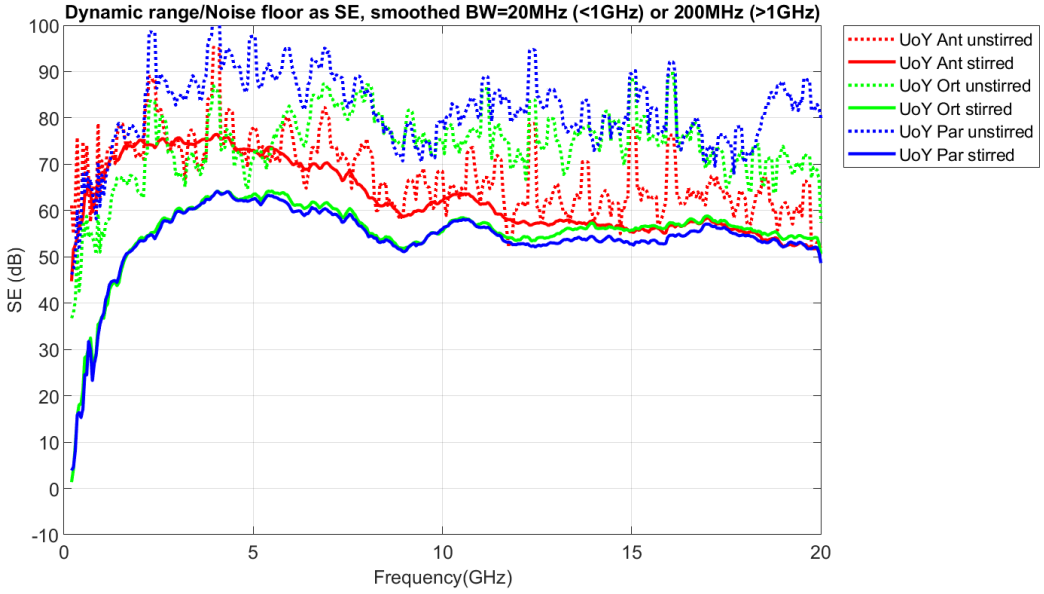

Figure 9. Dynamic range for the different measurement techniques (lin scale)

3. SE Measurements

Samples were soldered in place on the test jig at the castellation points so the solder connection around the edge is not continuous. This replicates the intended attachment. Samples 3 and 7 are not measured as they are too small to fit over the stripline.

Results for Sample 1 are shown in Figs 10 to Fig 19. At the lower part of the frequency range all measures of SE are in the range 30dB to 40dB. At higher frequencies, 10GHz and above, the SE values reduce to below 20dB. At some frequencies the SE has negative dB values commensurate with coupling enhancement. In some cases structure becomes apparent in the curves, which is indicative of resonant behavior.

The Stirred SE measurements for the parallel and orthogonal cases follow the dynamic range data at the lower frequencies where the dynamic range is low.

The data has been averaged as a power ratio using a rectangular window of 20 MHz at frequencies below 1 GHz and a rectangular window of 200 MHz at frequencies above 1 GHz. This makes it somewhat easier to see the separate curves.

The noise floor (NF) for each case, is plotted as a limiting shielding value for each measurement case. It is allowed to run off the top of the graph when it is well above the shielding effectiveness to best represent the shielding curves.

3.1 Sample 1

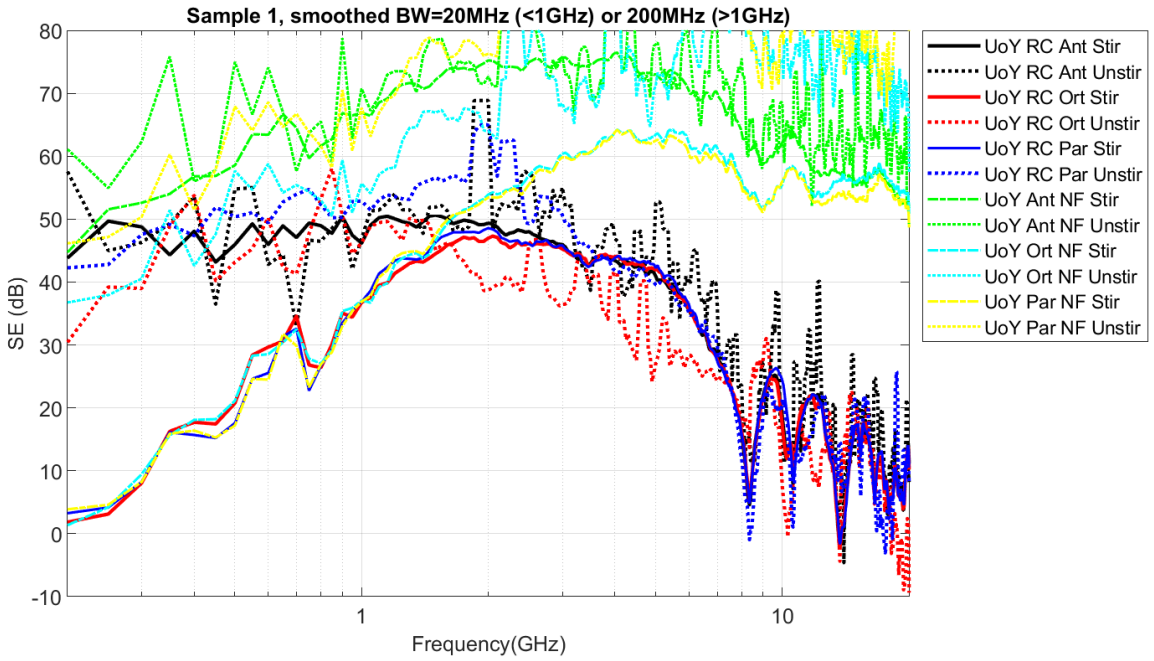

Figure 10. Sample 1 SE and noise floor as SE (log scale)

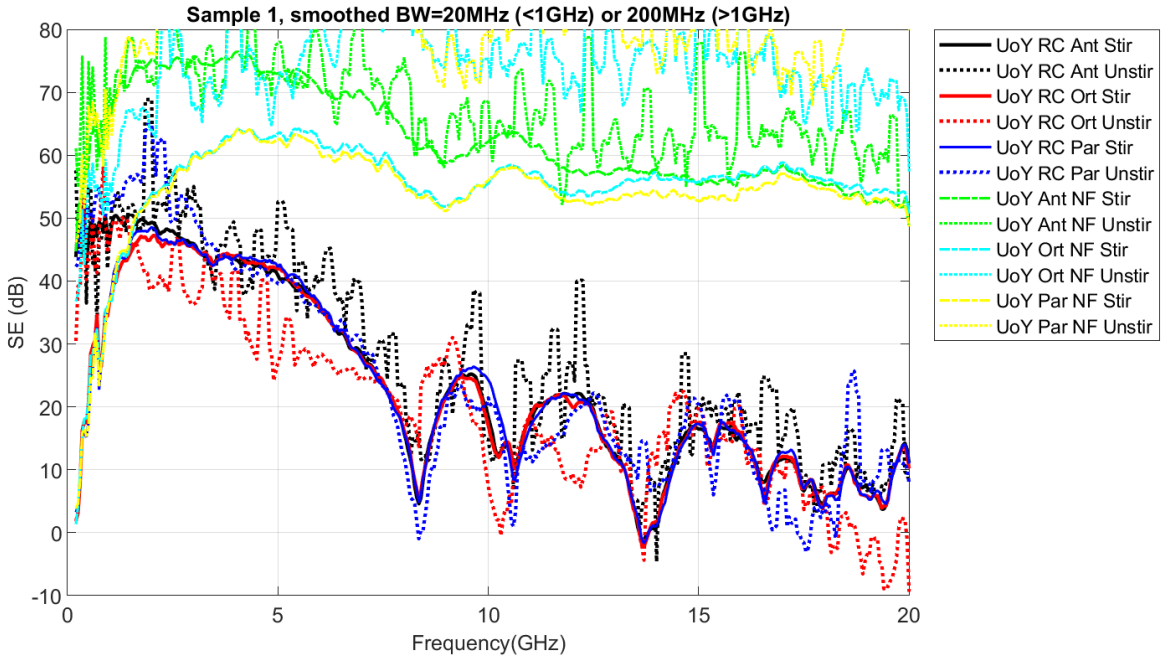

Figure 11. Sample 1 SE and noise floor as SE (lin scale)

3.2 Sample 2

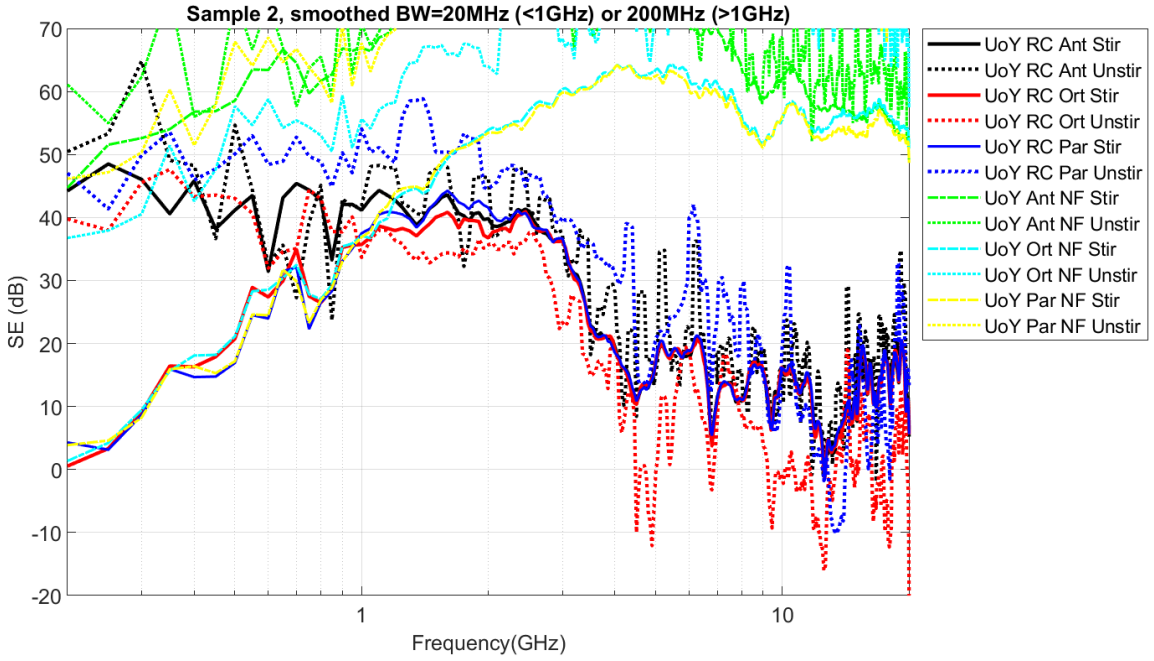

Figure 12. Sample 2 SE and noise floor as SE (log scale)

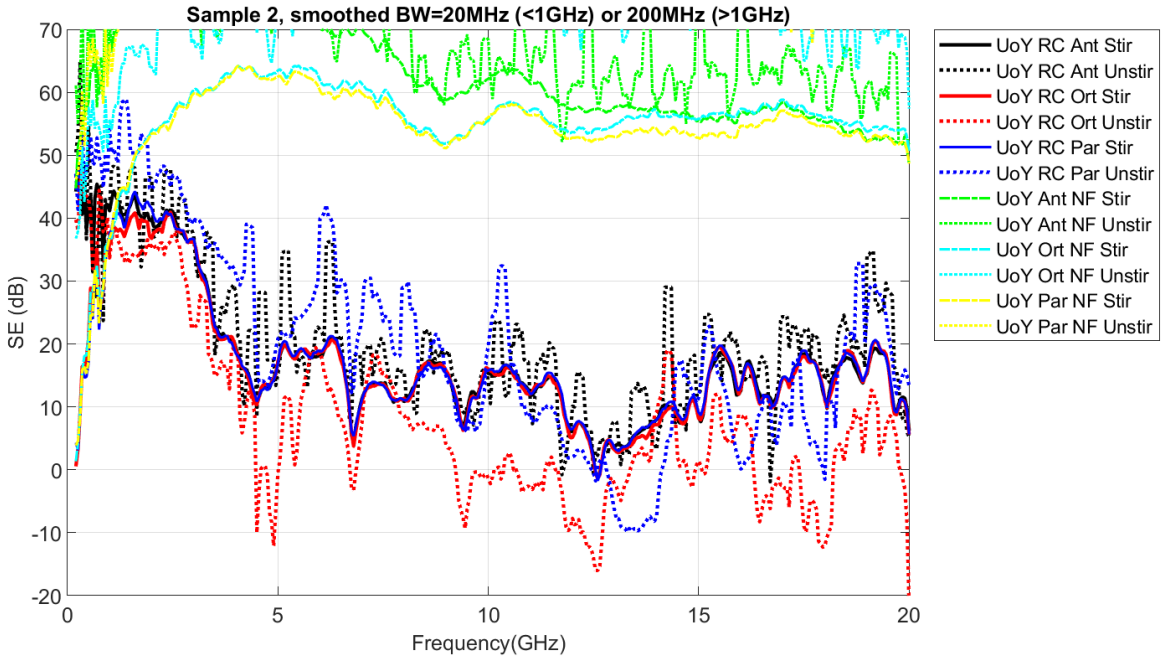

Figure 13. Sample 2 SE and noise floor as SE (lin scale)

3.3 Sample 3

Sample 3 was too small to fit the UoY prototype jig.

3.4 Sample 4

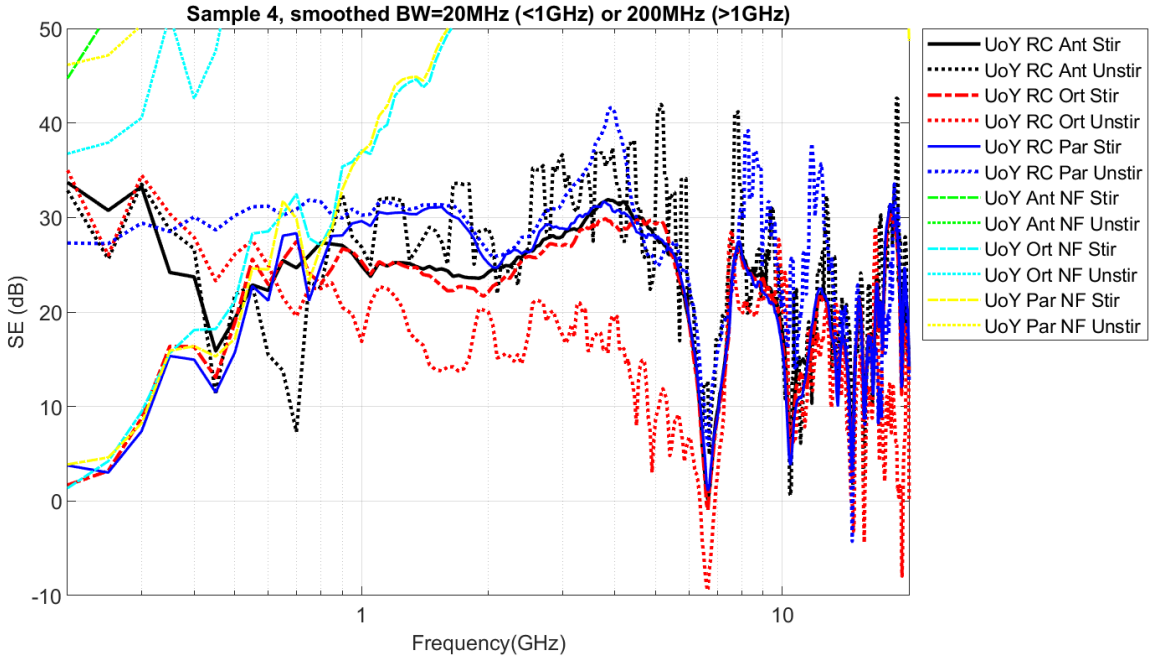

Figure 14. Sample 4 SE and noise floor as SE (log scale)

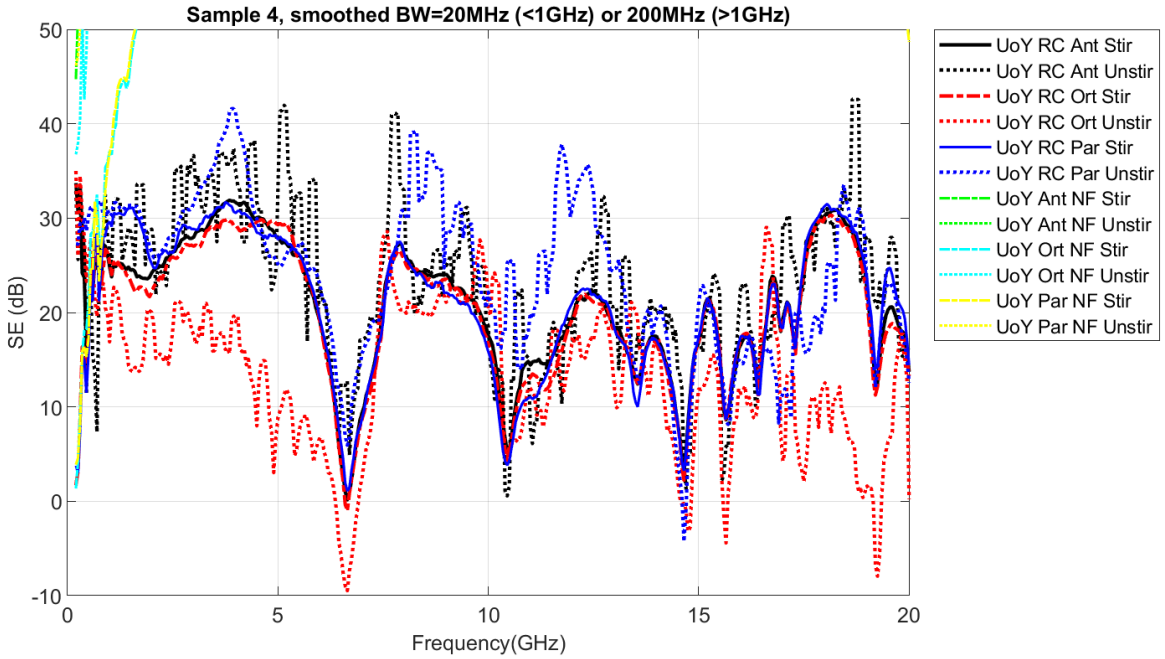

Figure 15. Sample 4 SE and noise floor as SE (lin scale)

3.5 Sample 5

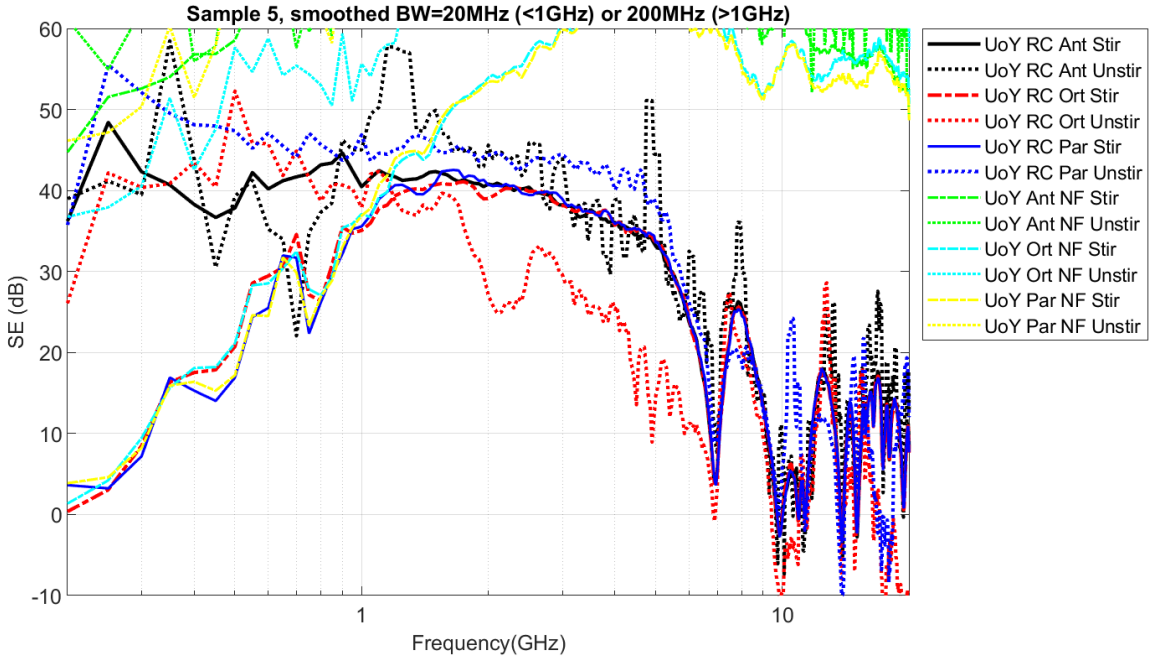

Figure 16. Sample 5 SE and noise floor as SE (log scale)

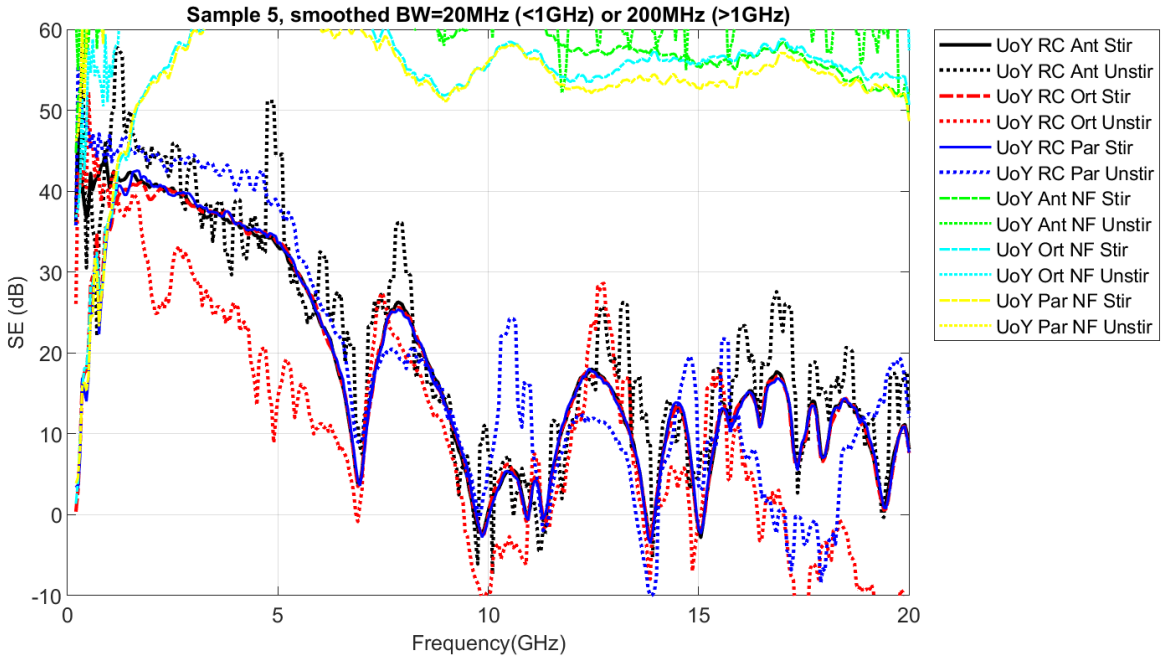

Figure 17. Sample 5 SE and noise floor as SE (log scale)

3.6 Sample 6

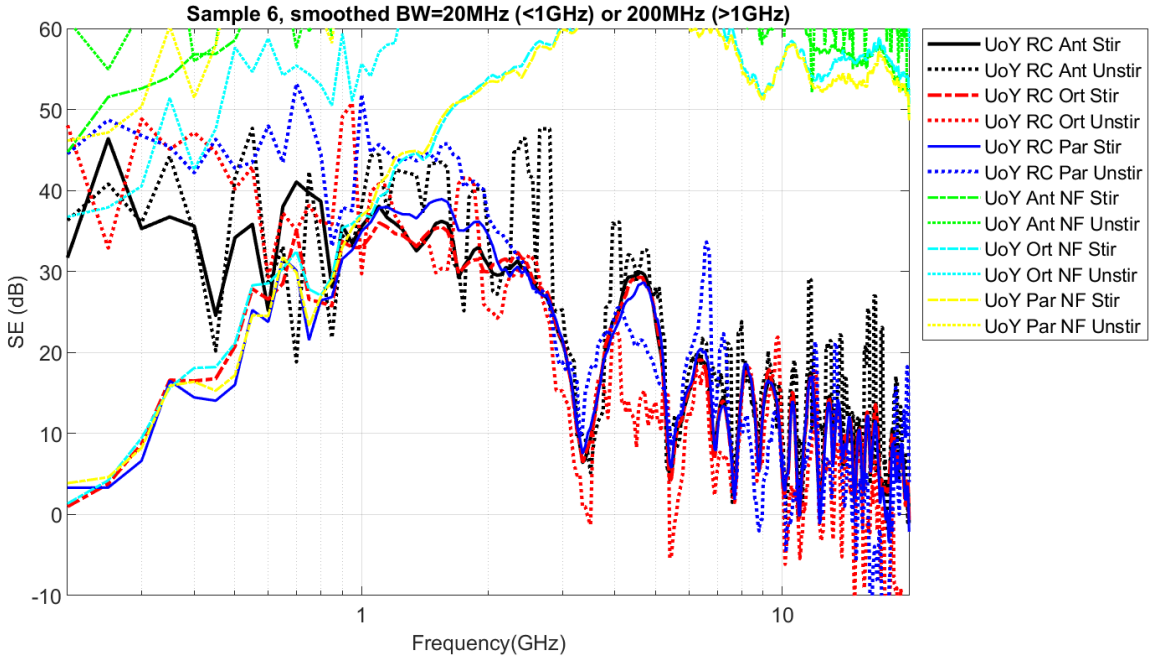

Figure 18. Sample 6 SE and noise floor as SE (log scale)

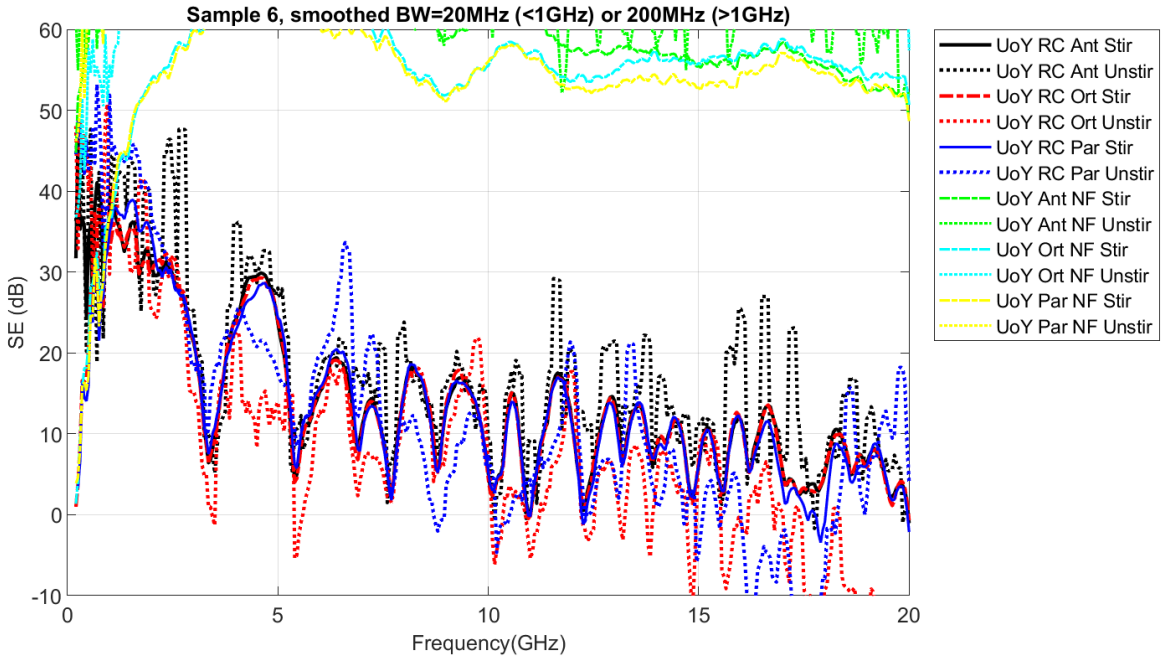

Figure 19. Sample 6 SE and noise floor as SE (log scale)

3.7 Sample 7

Sample 7 was too small to fit to the UoY prototype jig.

4. Concluding Remarks

We have defined two SE measurement types for board level shields, stirred and unstirred and performed a set of measurements using both antenna to shield and adjacent strip-line to shield coupling for each type. The results show the expected detail differences between the measurements, however the overall levels of SE are similar for each case. This was unexpected and as yet we have no explanation for this. Most of the shields have small apertures and castellated connections to the ground plane. These features explain the reduction in SE observed in all cases at the higher part of the frequency range.

Further consideration of the measurement technique after these results were obtained has resulted in a proposed SE measurement technique that may show the variability in SE of these shields when they are deployed in differing outer enclosures. This technique is currently being investigated experimentally as a development of the Stirred SE measurement described in 1.4.2. above and will be reported on when results are available.

References

[1] J. Clegg, A.C. Marvin, J.F. Dawson, and S.J. Porter, “Optimization of stirrer designs in a reverberation chamber,” *IEEE Transactions on Electromagnetic Compatibility*, vol. 47, 2005, pp. 824–832.

[2] A.C. Marvin, G. Esposito, J.F. Dawson, I.D. Flintoft, L. Dawson, J.A.K. Everard, and G.C.R. Melia, “A wide-band hybrid antenna for use in reverberation chambers,” *Electromagnetic Compatibility (EMC), 2013 IEEE International Symposium on*, Denver, Colorado: 2013, pp. 222–226.